A Residual-of-Residual Test of NFW Geometry in the Missing-Mass Problem

J. R. Landers

May 2026

Abstract

This short note applies the geometric-residual framework of Landers [1] to the simplest cold-dark-matter baseline: a pure Navarro-Frenk-White (NFW) halo. The question is not whether cold dark matter can be embedded in general relativity; it can. The sharper question is whether the weak-field residual geometry expected from a flat rotation curve is naturally reproduced by a pure NFW source. A synthetic flat-curve target from the parent warp-search experiment is fit with NFW, cored/isothermal, and log-potential residual families. NFW can match the outer flat part when fit only over the outer galaxy, but then it overpredicts the central residual. When fit over the full radial range, it loses the expected flat-curve acceleration slope. In residual language, the remaining "residual of the residual" is a structured correction to the source geometry, not random noise.

1. Question

The parent paper [1] reframes the missing-mass problem as an inverse problem over spacetime residuals. Instead of asking first which named theory is correct, it asks which geometric perturbation must be added to the baryon-predicted metric:

$$g_{\mu\nu}^{\rm trial} = g_{\mu\nu}^{\rm bar} + h_{\mu\nu}. \tag{1}$$

The relativistic residual is

$$\Delta G_{\mu\nu} := G_{\mu\nu}[g^{\rm obs}] - G_{\mu\nu}[g^{\rm bar}], \qquad T_{\mu\nu}^{\rm miss} := \frac{c^4}{8\pi G}\Delta G_{\mu\nu}. \tag{2}$$

If ordinary general relativity is retained, then a dark-matter model is a candidate stress-energy source for this residual.

For galaxies in the weak-field, nonrelativistic limit,

$$\mathrm{d}s^2 \simeq -\left(1+\frac{2\Phi}{c^2}\right)c^2\mathrm{d}t^2 + \left(1-\frac{2\Psi}{c^2}\right)\mathrm{d}\mathbf{x}^2, \tag{3}$$

and circular speeds primarily constrain Φ:

$$v^2(r) = r\frac{\mathrm{d}\Phi}{\mathrm{d}r}. \tag{4}$$

The practical residual used here is therefore

$$\boxed{\Delta g(r) = g_{\rm obs}(r) - g_{\rm bar}(r) = \frac{v_{\rm obs}^2(r) - v_{\rm bar}^2(r)}{r}.} \tag{5}$$

In a spherical diagnostic reduction, this residual defines

$$M_{\rm eff}(<r) = \frac{r^2\Delta g(r)}{G}, \qquad \rho_{\rm eff}(r) = \frac{1}{4\pi G r^2}\frac{\mathrm{d}}{\mathrm{d}r}\left[r^2\Delta g(r)\right]. \tag{6}$$

This note tests a narrow scientific claim: after the best pure NFW fit, what geometry is still missing? Define

$$\boxed{\epsilon_g(r) = \Delta g_{\rm target}(r) - \Delta g_{\rm NFW}(r),} \tag{7}$$

and its corresponding effective density proxy

$$\boxed{\epsilon_\rho(r) = \frac{1}{4\pi G r^2}\frac{\mathrm{d}}{\mathrm{d}r}\left[r^2\epsilon_g(r)\right].} \tag{8}$$

This is the residual of the residual: the part of the inferred geometry not explained by the selected physical source.

2. NFW in Residual Space

The NFW density profile [2] is

$$\rho_{\rm NFW}(r) = \frac{\rho_s}{(r/r_s)(1+r/r_s)^2}. \tag{9}$$

With $x = r/r_s$, the enclosed mass is

$$M_{\rm NFW}(<r) = 4\pi\rho_s r_s^3 \left[\ln(1+x) - \frac{x}{1+x}\right]. \tag{10}$$

The corresponding weak-field residual acceleration is

$$\Delta g_{\rm NFW}(r) = \frac{GM_{\rm NFW}(<r)}{r^2}. \tag{11}$$

This is a direct source-side prediction for the residual, once the two halo parameters are fixed.

A flat rotation residual asks for a different shape over the flat part of the curve:

$$v_{\rm extra}^2 \simeq v_f^2 \quad \Rightarrow \quad \Delta g_{\rm target}(r) \simeq \frac{v_f^2}{r}, \qquad \delta\Phi_{\rm target} \simeq v_f^2 \log r. \tag{12}$$

Thus the expected acceleration slope is

$$\frac{{\rm d}\ln \Delta g_{\rm target}}{{\rm d}\ln r} \simeq -1. \tag{13}$$

For NFW, writing

$$f(x) = \ln(1+x) - \frac{x}{1+x}, \tag{14}$$

the local acceleration slope is

$$\boxed{\frac{{\rm d}\ln \Delta g_{\rm NFW}}{{\rm d}\ln r} = \frac{x^2}{(1+x)^2 f(x)} - 2.} \tag{15}$$

This equals -1 only near $x \simeq 2.16$. It remains in the loose flat-curve band $-1.15 < s < -0.85$ only over $1.45 \lesssim x \lesssim 3.32$, about 0.36 dex in radius. NFW can therefore mimic a logarithmic-potential residual over a finite scale-radius band, but not as a general residual geometry.

3. Experiment

The target is the synthetic flat-curve residual from the geometry-first warp search of Landers [1]. The baryonic profile is the same toy exponential-disk-inspired cumulative mass used there,

$$M_{\rm bar}(<r) = M_b\left[1 - e^{-r/R_d}\left(1 + \frac{r}{R_d}\right)\right], \qquad g_{\rm bar}(r) = \frac{GM_{\rm bar}(<r)}{r^2}. \tag{16}$$

The observed curve is generated by adding a flat-speed component,

$$v_{\rm obs}^2(r) = v_{\rm bar}^2(r) + \left[v_f\left(1 - e^{-r/r_f}\right)\right]^2, \tag{17}$$

with $v_f = 190$ in the toy velocity units and $r_f = 4.5$ in the toy radial units. The resulting target residual rises through the inner galaxy and approaches v_f^2/r in the outer region.

Three families were fit to $\Delta g_{\rm target}$:

$$\Delta g_{\rm NFW}(r) = \frac{GM_{\rm NFW}(<r)}{r^2}, \tag{18}$$

$$\Delta g_{\rm iso}(r) = \frac{v_0^2 r}{r^2 + r_c^2}, \tag{19}$$

$$\Delta g_{\rm log}(r) = \frac{A}{r + r_0}. \tag{20}$$

The cored/isothermal profile is included as a control because it is explicitly designed to approach $\Delta g \propto 1/r$ outside its core. The log-potential tail is included as a minimal two-parameter warp-like comparison. Fits were performed over four radial windows: the full 0.3–40 range, 1–15, 3–30, and 10–40. The key diagnostic is whether a model can match both the inner transition and the outer flat-curve residual without leaving a structured ϵ_g.

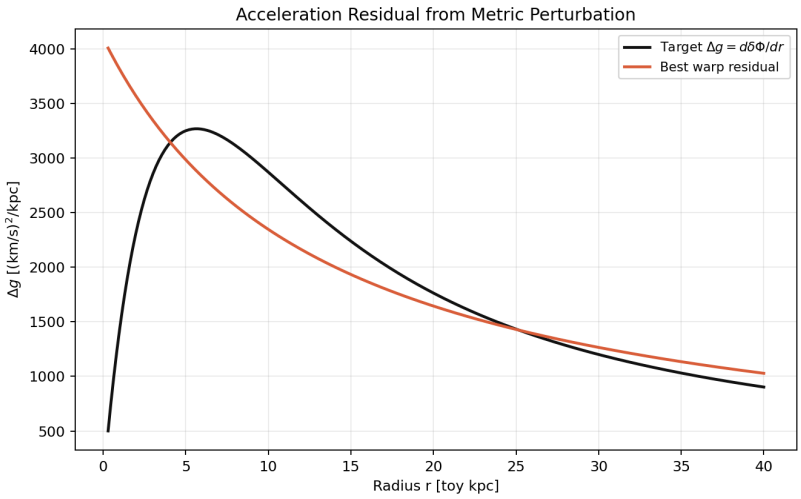

Figure 1: Target residual inherited from the parent warp search [1]. The synthetic flat-speed component produces an outer acceleration residual close to $\Delta g \propto 1/r$, equivalent to a logarithmic potential perturbation over the flat part of the curve.

Model	Fit range	Rel. RMSE	Mean frac. err.	Outer flat.	Outer slope	Near -1 frac.
NFW	0.3–40	0.258	0.213	0.102	-0.480	0.000
NFW	3–30	0.311	0.192	0.055	-0.744	0.301
NFW	10–40	0.504	0.231	0.025	-0.917	0.681
Cored/isothermal	0.3–40	0.031	0.020	0.028	-0.868	0.699

Table 1: Residual-space fits to the synthetic flat-curve target. "Outer slope" is the mean of $\mathrm{d}\ln\Delta g/\mathrm{d}\ln r$ over $10 \le r \le 40$. "Near -1 frac." is the fraction of outer points with slope between -1.15 and -0.85. The target has mean outer slope -0.891 and near--1 fraction 0.735.

4. Results

The experiment produces two complementary failures.

First, a full-range NFW fit spreads its scale radius outward:

$$\text{mass scale} = 257.84, \qquad r_s = 45.23. \tag{21}$$

This lowers the central overshoot, but the outer acceleration slope becomes too shallow. Over $10 \le r \le 40$, the mean NFW slope is -0.480, whereas the target slope is -0.891. None of the outer points are in the loose flat-curve slope band.

Second, an outer-only NFW fit chooses

$$\text{mass scale} = 52.29, \qquad r_s = 13.43. \tag{22}$$

This is the fit NFW wants if the task is only to match the flat tail. It gives outer flatness 0.025 and mean outer slope -0.917, almost exactly the expected logarithmic-potential residual. But the full relative RMSE worsens to 0.504 because the same NFW halo overpredicts the central residual by a large amount. In the residual-of-residual field, this appears as a negative inner source correction:

$$\epsilon_g(r) < 0 \quad \text{through most of the inner region.} \tag{23}$$

The corresponding ϵ_ρ is also negative over the central correction region. This is not a physical negative matter claim by itself; it is a diagnostic statement: after pure NFW is forced to explain the outer geometry, the remaining geometry asks for removal or redistribution of central source structure.

The cored/isothermal control demonstrates that the target is not hard to fit in residual space. Its full-range fit gives relative RMSE 0.031 and mean fractional error 0.020, with mean outer slope -0.868. This is expected:

$$\Delta g_{\mathrm{iso}}(r) = \frac{v_0^2 r}{r^2 + r_c^2} \longrightarrow \frac{v_0^2}{r} \quad (r \gg r_c). \tag{24}$$

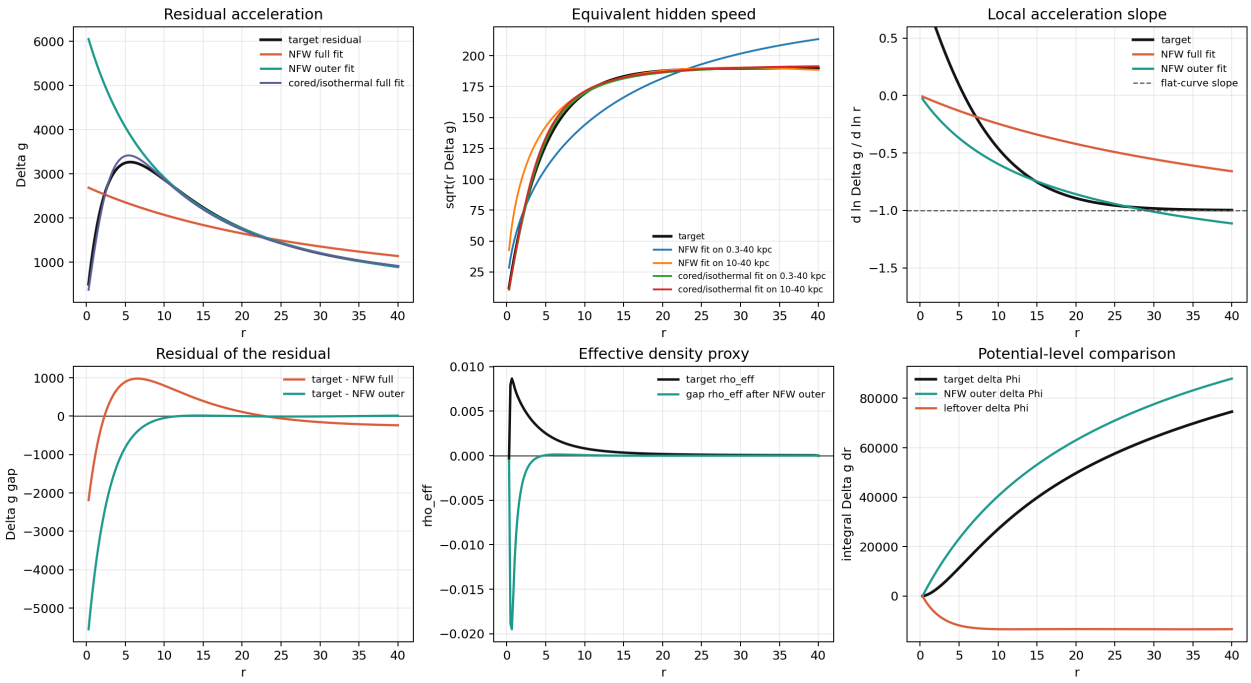

Figure 2: Residual-of-residual diagnostic for pure NFW. Top left: the full-range NFW fit misses the target shape, while the outer-range NFW fit matches the flat tail but overshoots the inner residual. Top middle and right: the outer NFW fit recovers the flat hidden speed and near--1 acceleration slope only over the outer range. Bottom left: the leftover $\epsilon_g = \Delta g_{\rm target} - \Delta g_{\rm NFW}$ is structured, not noise. Bottom middle: interpreted as an effective source correction, the leftover after the outer NFW fit is strongly negative in the inner region. Bottom right: the potential-level comparison shows that the outer NFW fit accumulates too much central potential before tracking the flat-curve tail.

The control is not presented as the correct theory. It is a shape test showing that the residual target prefers an extended, cored, nearly logarithmic potential structure over this radial range.

5. Interpretation

This result is the cusp/core tension expressed in the language of residual geometry [6]. Pure NFW is a valid stress-energy source inside general relativity, but its residual acceleration shape is not freely logarithmic. It has three characteristic regimes:

$$r \ll r_s : \rho \sim r^{-1}, \quad M(<r) \sim r^2, \quad \Delta g \sim \text{const}, \tag{25}$$

$$r \sim r_s : \Delta g \text{ can mimic } 1/r \text{ over a finite band}, \tag{26}$$

$$r \gg r_s : \rho \sim r^{-3}, \quad M(<r) \sim \log r, \quad \Delta g \sim \frac{\log r}{r^2}. \tag{27}$$

Therefore the NFW explanation of a flat rotation residual requires the observed flat region to align with the halo's scale-radius band. If the same profile is required to fit the inner transition, the alignment is lost.

The residual-of-residual object makes this failure useful rather than merely negative. A random residual would suggest noise or an underfit. A structured inner negative correction suggests a specific missing element: core formation, baryonic feedback, a non-NFW phase-space distribution, self-interactions, wave-like pressure, a modified source decomposition, or some systematic error in the target construction. The present experiment does not choose among those possibilities. It only says what the geometry asks for after pure NFW has done its best.

6. Limitations and Next Tests

This is a synthetic weak-field experiment, not a real galaxy fit. The inversion uses a spherical effective-density proxy, not a disk model. The target is built from a chosen flat-speed component rather than from SPARC data [4]. No cosmological halo-concentration prior is imposed. No lensing observable is fit. The diagnostic is therefore a controlled shape test, not evidence against cold dark matter as a full theory.

The immediate next step is to repeat the same residual-of-residual calculation on real rotation curves with disk geometry:

$$\epsilon_g(r) = \Delta g_{\text{inferred}}(r) - \Delta g_{\text{candidate}}(r), \tag{28}$$

then classify ϵ_g and ϵ_ρ across galaxies. If the leftover geometry clusters into repeated families, those families become stronger targets for physics: feedback-generated cores, self-interacting halos, ultralight scalar cores, warm-dark-matter phase-space limits, baryonic systematics, or modified-gravity terms.

7. Compact Conclusion

In the parent geometric-residual framework, the question is not just whether a dark-matter candidate exists. It is whether its stress-energy produces the observed residual geometry:

$$\Delta G_{\mu\nu} \stackrel{?}{=} \frac{8\pi G}{c^4} T_{\mu\nu}^{\text{candidate}}. \tag{29}$$

For the synthetic flat-curve target tested here, pure NFW/CDM gives a clear answer: it can match the outer logarithmic-potential residual, or it can reduce the inner overshoot, but it does not naturally do both with one profile. The leftover field is structured and interpretable. That is the value of the residual-of-residual test: it turns a familiar model mismatch into an explicit geometric object that can be compared across candidate physics.

References

[1] Landers, J. R. (2026). Geometric residuals and weak-field warp search in the missing-mass problem. Unpublished manuscript, May 2026.

[2] Navarro, J. F., Frenk, C. S., & White, S. D. M. (1996). The structure of cold dark matter halos. *The Astrophysical Journal*, 462, 563–575. doi:10.1086/177173.

[3] Rubin, V. C., Ford, W. K., Jr., & Thonnard, N. (1980). Rotational properties of 21 Sc galaxies with a large range of luminosities and radii. *The Astrophysical Journal*, 238, 471–487. doi:10.1086/158003.

[4] Lelli, F., McGaugh, S. S., & Schombert, J. M. (2016). SPARC: Mass models for 175 disk galaxies with Spitzer photometry and accurate rotation curves. *The Astronomical Journal*, 152, 157. doi:10.3847/0004-6256/152/6/157.

[5] McGaugh, S. S., Lelli, F., & Schombert, J. M. (2016). The radial acceleration relation in rotationally supported galaxies. *Physical Review Letters*, 117, 201101. doi:10.1103/PhysRevLett.117.201101.

[6] de Blok, W. J. G. (2010). The core-cusp problem. *Advances in Astronomy*, 2010, 789293. doi:10.1155/2010/789293.

[7] Bertone, G., & Hooper, D. (2018). History of dark matter. *Reviews of Modern Physics*, 90, 045002. doi:10.1103/RevModPhys.90.045002.